PERGAMON

International Journal of Heat and Mass Transfer 43 (2000) 4217–4227

International Journal of HEAT and MASS TRANSFER

www.elsevier.com/locate/ijhmt

High temperature contact conductance measurement across cylindrical joint by the periodic method: feasibility and first results

P. Benigni [a,b,*], C. Marchionni [a], J. Rogez [b]

[a] *Département Physico-Chimie, I.R.S.I.D., Voie Romaine, BP 320, F-57214 Maizières-les-metz Cedex, France*
[b] *Centre de Thermodynamique et Microcalorimétrie du C.N.R.S., 26 Rue du 141ème R.I.A., F-13331 Marseille Cedex 3, France*

Received 26 June 1999; received in revised form 18 February 2000

Abstract

This paper deals with the possibility and the first measurements of thermal contact conductance of cylindrical joints by the periodic method at high temperature. The mathematical principle is presented. The calibration of the method is performed on a composite nickel/nickel cylinder, the interface of which has a controlled macroroughness. The experimental results are compared with the results of a geometric conductance model. A good agreement is observed.

1. Introduction

The heat transfer in a structure built from several elements in contact does not only depend on the thermal properties of each unit element, but also on the quality of the thermal contact between them. The study of thermal contacts has received an increasing interest in recent literature [1] as it becomes more and more important in numerous applications like high density microelectronics, composite materials, solidification processes, accurate contact temperature measurements etc. The heat transfer across a contact is classically represented by a contact conductance coefficient, which is defined, in steady-state, as the ratio of the heat flow density to the temperature drop at the interface.

Experimental setups designed for contact conductance measurements generally feature a cylindrical sample made of two cylinders in contact along their bases. The test sample is placed between a heat source and a heat sink in a vertical cylindrical column which undergoes an axial steady temperature gradient and an axial load. Two series of thermocouples in the column allows the temperature distribution in each part of the sample to be known. By knowing the thermal conductivities of the materials brought in contact, the heat flow can be calculated. The temperature drop at the interface is obtained by extrapolation of the two bulk temperature distributions. The contact conductance is then easily worked out from the definition.

Methods based on a thermal regime where the temperature varies with time are considerably less used. Among them, the early works of Laurent et al. [2], illustrate one of the applications of the well known flash method to contact conductance measurementss. The periodic method has also been used. Close to the original Angström method [3], the works of Saint-Blanquet

* Corresponding author. Tel.: +33-03-87-70-48-23; fax: +33-03-87-70-41-14.
E-mail addresses: pierre.benigni@irsid.usinor.com (P. Benigni), jrz@ctm.cnrs-mrs.com (J. Rogez).

0017-9310/00/$ - see front matter
PII: S0017-9310(00)00069-7

Nomenclature

a	distance between the axis of the cylinder and the interface in the composite sample
Arg	argument of a complex number
b	distance between the axis of the cylinder and the outer thermocouple
ber	Kelvin function of zero order, real part of I_0
bei	Kelvin function of zero order, imaginary part of I_0
Bi	Biot number, $=a{\cdot}h/\lambda$
c	radius of the cylindrical sample
C_p	heat capacity
e	inverse of the thermal diffusion length, $=\sqrt{\omega/\alpha}$
I_0	modified Bessel function I of zero order
K_0	modified Bessel function K of zero order
ker	modified Kelvin function of zero order, real part of K_0
kei	modified Kelvin function of zero order, imaginary part of K_0
Mod	modulus of a complex number
P	period of the thermal wave
r	radial coordinate
t	time
T	temperature
α	thermal diffusivity
φ	argument of the temperature
Φ	phase change of the temperature
λ	thermal conductivity
h	contact conductance
θ	amplitude of the temperature
ρ	density
ω	angular velocity

and Bardon [4], Robinson and Tomsic [5], and Cordier et al. [6] involve long cylindrical samples. Their setups allow the conductance measurements to be performed under both, steady and periodic states for comparison. It is shown that the accuracy under periodic regime is comparable to that under steady flow. More recently, Nguyen-Minh and Neuer [7] have demonstrated the applicability of the Cowan's method [8], for the measurement of the contact conductance of a two-layer disk shaped sample.

All the above mentioned methods deal with plane contacts, on the other hand the cylindrical joints are considerably less commonly studied [9–10]. Madhusudana and Litvak [11] mention that "there were only a half-dozen works dealing specifically with cylindrical joints compared with more than 150 studies on flat joints" during the seventies. To the extent that cylindrical contacts occur very often in engineering applications, it can be concluded that specific studies are needed.

As no previous work has been found concerning the application of the periodic method for conductance measurement across a cylindrical joint, at first, the mathematical basis of the method is exposed.

2. Mathematical basis of the measurement

In the classical Angström method, the amplitude ratio and the phase change of the thermal wave (strictly speaking this is not a wave but the term will be thus employed in the following) between the two measurement points, are explicit functions of the thermal diffusivity. In this part, the aim is to find out similar functions which connect the amplitude ratio or the phase change of the thermal wave to the contact conductance.

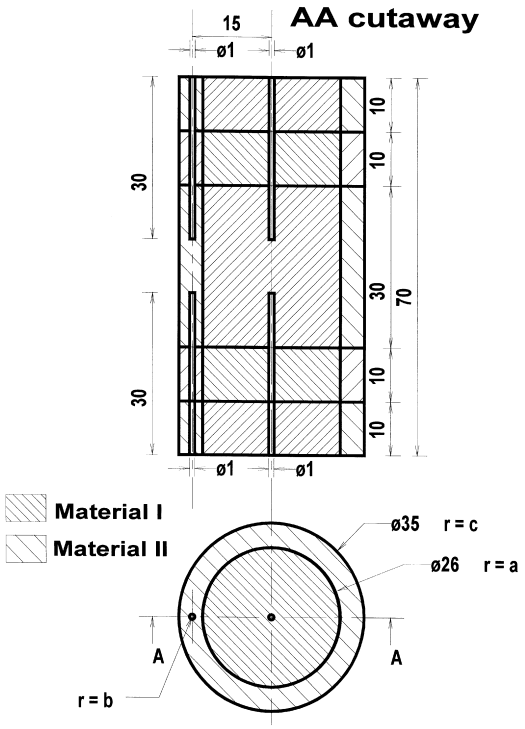

Fig. 1. Sample composite cylinder showing the holes of $\phi\,1\times10^{-3}$ m at $r=0$ and $r=b$ in which are inserted the hot junctions of the thermocouple circuit. Dimensions in 10^{-3} m.

Fig. 1 shows the composite cylindrical sample. The material I extends from the center (r = 0) to the interface position ($r = a$). The material II extends from the interface ($r = a$) to the sample radius ($r = c$). The inner and outer thermocouples are located at ($r = 0$) and ($r = b$), respectively ($a < b < c$). The thermal conductivities and thermal diffusivities of the two materials in contact are denoted by λ_I, λ_{II}, α_I, α_{II}, respectively. In cylindrical coordinates, assuming that the heat transfer is 1D, the temperature (T) only depends on the radial distance (r) and the time (t). Then the system of differential equations (1) and (2) is to be solved:

$$0 \le r \le a: \qquad \frac{\partial^2 T}{\partial r^2} + \frac{1}{r}\frac{\partial T}{\partial r} - \frac{1}{\alpha_I}\frac{\partial T}{\partial t} = 0 \tag{1}$$

$$a \le r \le c: \qquad \frac{\partial^2 T}{\partial r^2} + \frac{1}{r}\frac{\partial T}{\partial r} - \frac{1}{\alpha_{II}}\frac{\partial T}{\partial t} = 0 \tag{2}$$

The sample surface is heated periodically at ($r = c$) with the angular velocity (ω). The amplitude of the oscillation at the location of the outer thermocouple ($r = b$) is denoted by ($\theta(b)$). Hence, the boundary condition is written as:

$$T(b, t) = \theta(b)\cos \omega t \tag{3}$$

At the interface, the heat transfer is described by the thermal contact conductance coefficient (h). A mathematical discontinuity of the temperature field is introduced, the magnitude of which is proportional to the heat flow yielding the system of equations (4) and (5):

$$\lambda_I\left(\frac{\partial T}{\partial r}\right)_{r=a^-} = h\big(T(a_+) - T(a_-)\big) \tag{4}$$

$$\lambda_{II}\left(\frac{\partial T}{\partial r}\right)_{r=a^+} = h\big(T(a_+) - T(a_-)\big) \tag{5}$$

Eqs. (4) and (5) are based on the assumption that the contact conductance, defined formally under steady heat flow, is still valid under periodic heat flow. According to Robinson and Tomsic [5], transient corrections are necessary only for a time scale of 0.1 s, which is less than the range of periods used in this study (60–650 s). In the works of Cordier et al. [6], five models of contact conditions featuring different setups of resistances and capacities in series or parallel are correlated with experimental results. In the range of period (30–500 s), the simple contact conductance model was found to be the only one which fits the experimental results well. The introduction of an additional thermal capacity in the contact conditions is discussed by Fourcher et al. [12]. These authors show that, in fact, it is necessary to introduce a lack of thermal capacity because the heat capacities of the materials in contact are generally greater than the heat capacity of the interstitial medium. In the following, the simple conductance scheme will be used to the extent that the capacity effect must represent only a weak correction, the magnitude of which is certainly smaller than the magnitude of the experimental errors in the present setup.

In the above equations, the parameters (λ_I, λ_{II}, α_I, α_{II}, a, b, ω) are supposed to be known quantities. The conductance (h) is sought as a function of the amplitude ratio $\Theta = \theta(0)/\theta(b)$ and the phase change $\Phi = \varphi(0) - \varphi(b)$ of the periodic temperature, which are worked out from digital Fourier transform of the temperature recordings at ($r = 0$) and ($r = b$).

In the periodic state, a complex temperature is defined as: $T^*(r, t) = \theta^*(r) \cdot \exp(i\omega t)$, where ($\theta^*(r)$) is a complex amplitude. The real part of (T^*) represents the physical temperature. The reciprocal thermal diffusion lengths in the two materials are denoted by: $e_I = \sqrt{\omega/\alpha_I}$, $e_{II} = \sqrt{\omega/\alpha_{II}}$. Eqs. (1)–(5) can be put in the form:

$$\frac{\partial^2 \theta^*}{\partial r^2} + \frac{1}{r}\frac{\partial \theta^*}{\partial r} - i \cdot e_I^2 \cdot \theta^* = 0 \tag{6}$$

$$\frac{\partial^2 \theta^*}{\partial r^2} + \frac{1}{r}\frac{\partial \theta^*}{\partial r} - i \cdot e_{II}^2 \cdot \theta^* = 0 \tag{7}$$

$$T^*(b, t) = \theta(b) \cdot \exp(i\omega t) \tag{8}$$

$$\lambda_I\left(\frac{\partial \theta^*}{\partial r}\right)_{r=a^-} = h\big(\theta^*(a_+) - \theta^*(a_-)\big) \tag{9}$$

and

$$\lambda_{II}\left(\frac{\partial \theta^*}{\partial r}\right)_{r=a^+} = h\big(\theta^*(a_+) - \theta^*(a_-)\big) \tag{10}$$

Relations (6) and (7) are Bessel equations which admit solutions in the form:

$$\theta^{*I}(r) = A \cdot I_0\big(e_I \cdot r \cdot i^{1/2}\big) + B \cdot K_0\big(e_I \cdot r \cdot i^{1/2}\big) \tag{11}$$

$$\theta^{*II}(r) = C \cdot I_0\big(e_{II} \cdot r \cdot i^{1/2}\big) + D \cdot K_0\big(e_{II} \cdot r \cdot i^{1/2}\big) \tag{12}$$

where (I_0) and (K_0) are the modified Bessel functions of zero order. $K_0(x)$ tends to infinity as x approaches (0), which implies that the coefficient (B) in Eq. (11) equals zero. The three remaining unknown coefficients (A, C, D) can be deduced from Eqs. (8–10). For writing simplification, let the Bessel functions and the first derivatives be denoted by:

$$I_r^I = I_0\big(e_I \cdot r \cdot i^{1/2}\big) \qquad I'^{I}_{r} = I'_0\big(e_I \cdot r \cdot i^{1/2}\big)$$

$$I_r^{\mathrm{II}} = I_0\left(e_{\mathrm{II}} \cdot r \cdot i^{1/2}\right) \qquad I'^{\,\mathrm{II}}_{\,r} = I'_0\left(e_{\mathrm{II}} \cdot r \cdot i^{1/2}\right)$$

$$K_r^{\mathrm{II}} = K_0\left(e_{\mathrm{II}} \cdot r \cdot i^{1/2}\right) \qquad K'^{\,\mathrm{II}}_{\,r} = K'_0\left(e_{\mathrm{II}} \cdot r \cdot i^{1/2}\right)$$

Substitution in Eqs. (11) and (12) yields:

$$\theta^{*\mathrm{I}}(r) = A \cdot I_r^{\mathrm{I}} \tag{13}$$

$$\theta^{*\mathrm{II}}(r) = C \cdot I_r^{\mathrm{II}} + D \cdot K_r^{\mathrm{II}} \tag{14}$$

and in Eq. (8):

$$\theta^{*\mathrm{II}}(b) = \theta(b) \tag{15}$$

Substitution of Eqs. (13) and (14) into Eqs. (9), (10) and (15), using the notations $\gamma_{\mathrm{I}} = e_{\mathrm{I}} \cdot \lambda_{\mathrm{I}} \cdot i^{1/2}$ and $\gamma_{\mathrm{II}} = e_{\mathrm{II}} \cdot \lambda_{\mathrm{II}} \cdot i^{1/2}$, gives:

$$\gamma_{\mathrm{I}} \cdot A \cdot I'^{\,\mathrm{I}}_{\,a} = h\left(C \cdot I_a^{\mathrm{II}} + D \cdot K_a^{\mathrm{II}} - A \cdot I_a^{\mathrm{I}}\right) \tag{16}$$

$$\gamma_{\mathrm{II}} \cdot \left(C \cdot I'^{\,\mathrm{II}}_{\,a} + D \cdot K'^{\,\mathrm{II}}_{\,a}\right) = h\left(C \cdot I_a^{\mathrm{II}} + D \cdot K_a^{\mathrm{II}} - A \cdot I_a^{\mathrm{I}}\right) \tag{17}$$

$$\theta(b) = C \cdot I_b^{\mathrm{II}} + D \cdot K_b^{\mathrm{II}} \tag{18}$$

These simultaneous equations are put in matrix form:

$$\begin{bmatrix} 0 & I_b^{\mathrm{II}} & K_b^{\mathrm{II}} \\ \gamma_{\mathrm{I}} \cdot I'^{\,\mathrm{I}}_{\,a} + h \cdot I_a^{\mathrm{I}} & -h \cdot I_a^{\mathrm{II}} & -h \cdot K_a^{\mathrm{II}} \\ h \cdot I_a^{\mathrm{I}} & \gamma_{\mathrm{II}} \cdot I'^{\,\mathrm{II}}_{\,a} - h \cdot I_a^{\mathrm{II}} & \gamma_{\mathrm{II}} \cdot K'^{\,\mathrm{II}}_{\,a} - h \cdot K_a^{\mathrm{II}} \end{bmatrix} \begin{bmatrix} A \\ C \\ D \end{bmatrix} = \begin{bmatrix} \theta(b) \\ 0 \\ 0 \end{bmatrix} \tag{19}$$

The determinant of the 3×3 square matrix is then:

$$\mathrm{Det} = \gamma_{\mathrm{I}} \cdot \gamma_{\mathrm{II}} \cdot I'^{\,\mathrm{I}}_{\,a}\left(I'^{\,\mathrm{II}}_{\,a} \cdot K_b^{\mathrm{II}} - I_b^{\mathrm{II}} \cdot K'^{\,\mathrm{II}}_{\,a}\right) + h \cdot (\gamma_{\mathrm{II}} \cdot I_a^{\mathrm{I}}\left(I'^{\,\mathrm{II}}_{\,a} \cdot K_b^{\mathrm{II}} - I_b^{\mathrm{II}} \cdot K'^{\,\mathrm{II}}_{\,a}\right) + \gamma_{\mathrm{I}} \cdot I'^{\,\mathrm{I}}_{\,a}\left(I_b^{\mathrm{II}} \cdot K_a^{\mathrm{II}} - I_a^{\mathrm{II}} \cdot K_b^{\mathrm{II}}\right) \tag{20}$$

The amplitude and the phase of the temperature at the center of the sample are respectively the module and the argument of the complex temperature at $(r = 0)$: $I_0(0) = 1$, hence $\theta^{*\mathrm{I}}(0) = A$ and $T^*(0,\ t) = A \cdot \exp(i\omega t)$. Thus, (Θ) and (Φ) are independent of (C) and (D), as a consequence, we are only interested in solving for (A) in the system (19):

$$A = \frac{1}{\mathrm{Det}} \begin{vmatrix} \theta(b) & I_b^{\mathrm{II}} & K_b^{\mathrm{II}} \\ 0 & -h \cdot I_a^{\mathrm{II}} & -h \cdot K_a^{\mathrm{II}} \\ 0 & \gamma_{\mathrm{II}} \cdot I'^{\,\mathrm{II}}_{\,a} - h \cdot I_a^{\mathrm{II}} & \gamma_{\mathrm{II}} \cdot K'^{\,\mathrm{II}}_{\,a} - h \cdot K_a^{\mathrm{II}} \end{vmatrix} \tag{21}$$

Calculating the determinant in Eq. (21) yields:

$$A = \theta(b) \cdot \frac{\gamma_{\mathrm{II}}.h}{\mathrm{Det}}\left(I'^{\,\mathrm{II}}_{\,a} \cdot K_a^{\mathrm{II}} - I_a^{\mathrm{II}} \cdot K'^{\,\mathrm{II}}_{\,a}\right) \tag{22}$$

Using the Wronskian relation [13]:

$$I'_v(z) \cdot K_v(z) - I_v(z) \cdot K'_v(z) = \frac{1}{z} \quad \forall v,\ z \neq 0$$

where $z = e_{\mathrm{II}} \cdot a \cdot i^{1/2}$, Eq. (22) reduces to:

$$A = \frac{\lambda_{\mathrm{II}} \cdot h \cdot \theta(b)}{a \cdot \mathrm{Det}} \tag{23}$$

The measurement of the amplitude ratio (Θ) between $(r = 0)$ and $(r = b)$ allows one to deduce (h) from Eq. (23):

$$\theta(0) = \mathrm{Mod}\left(T^*(0,\ t)\right) = \mathrm{Mod}(A) = \frac{\lambda_{\mathrm{II}} \cdot h \cdot \theta(b)}{a \cdot \mathrm{Mod(Det)}}$$

$$h = \frac{1}{\lambda_{\mathrm{II}}} \cdot \Theta \cdot a \cdot Mod(Det) \tag{24}$$

Eq. (20) shows off that the determinant is a linear function of (h), its module can be written as: $\mathrm{Mod(Det)} = \sqrt{a_2 \cdot h^2} + a_1 \cdot h + a_0$. Squaring Eq. (24) yields an equation of the second degree in (h). Only the positive root have a physical significance.

The phase of the temperature at the center of the sample is:

$$\varphi(0) = \mathrm{Arg}\left(T^*(0,\ t)\right) = \mathrm{Arg}(A) + \omega t$$
$$= -\mathrm{Arg(Det)} + \omega t \tag{25}$$

At $r = b$:$\varphi(b) = \omega t$, hence, the phase change (Φ) of the wave between $(r = b)$ and $(r = 0)$ is simply:

$$\Phi = -\mathrm{Arg}(A) = \mathrm{Arg(Det)} \tag{26}$$

The measurement of (Φ) gives a second equation from which (h) can be infered.

In the particular case of similar materials in contact, the notations can be reduced to:$\lambda_{\mathrm{I}} = \lambda_{\mathrm{II}} = \lambda$, $\alpha_{\mathrm{I}} = \alpha_{\mathrm{II}} = \alpha$, $e_{\mathrm{I}} = e_{\mathrm{II}} = e$, $\gamma_{\mathrm{I}} = \gamma_{\mathrm{II}} = \gamma$ and$I_r^{\mathrm{I}} = I_r^{\mathrm{II}} = I_r$, $K_r^{\mathrm{I}} = K_r^{\mathrm{II}} = K_r$, $I'^{\,\mathrm{I}}_{\,r} = I'^{\,\mathrm{II}}_{\,r} = I'_r$, $K'^{\,\mathrm{I}}_{\,r} = K'^{\,\mathrm{II}}_{\,r} = K'_r$.

Using the Wronskian relation again, the determinant now becomes:

$$\mathrm{Det} = \lambda\left(i \cdot \lambda \cdot e^2 \cdot I'_a\left(I'_a \cdot K_b - I_b \cdot K'_a\right) + \frac{h}{a} \cdot I_b\right) \tag{27}$$

By substituting Eq. (27) into Eq. (23), if the Biot dimensionless number is denoted by ($Bi = h \cdot a/\lambda$), the coefficient (A) is written in the form:

$$A = \frac{\theta(b) \cdot Bi}{(e \cdot a)^2 i \cdot I'_a\left(I'_a \cdot K_b - I_b \cdot K'_a\right) + Bi \cdot I_b} \tag{28}$$

Eq. (28) depends on three dimensionless numbers: (Bi), ($e{\cdot}a$) and ($e{\cdot}b$). For a perfect thermal contact, the conductance (h) and the Biot number (Bi) approach infinity. The first term in the denominator of the relation (28) is negligible towards the second one and (A) reduces to:

$$A = \frac{\theta(b)}{I_b^1} \tag{29}$$

Using Eq. (13), the complex temperature is written as: $T^*(r, t) = \theta(b) \cdot \frac{I_r^1}{I_b^1} \cdot \exp(i\omega t)$ which is the solution of the heat transfer equation for an infinite homogeneous cylinder under periodic boundary conditions.

3. Experiment

3.1. Apparatus

The experimental setup (Fig. 2) is the same as that for thermal diffusivity measurements [14], and will not be described again in detail. The main furnace controls the average temperature. The microfurnace power supply is modulated by a very low frequency generator (0.001–1 Hz) to give the AC component of the temperature. Inside the cylindrical sample ($H = 0.07$ m, $= 0.035$ m), the temperature is measured at the center ($r = 0$) and at the distance ($b = 0.015$ m) by means of split intrinsic Pt/Pt–Rh 10% thermocouples which are a requisite for measurements up to 1800 K. Taking into account that the radius c is imposed by the inner diameter of the microfurnace, the a and b distances have been optimized to allow the measurements of thermal resistances in the range 10^{-2}–10 W cm^2 K^{-1}. A digital scanner/voltmeter and a microcomputer allow to record and to process the electric response of the sensors. The axial heat flow is minimized in the sample in two ways: (i) Some axial thermal resistances are set up by cutting the sample in disks of various thicknesses as shown in Fig. 1. The height of the cylinder where the measurement is performed is optimized by the calculation previously published [15]. (ii) The

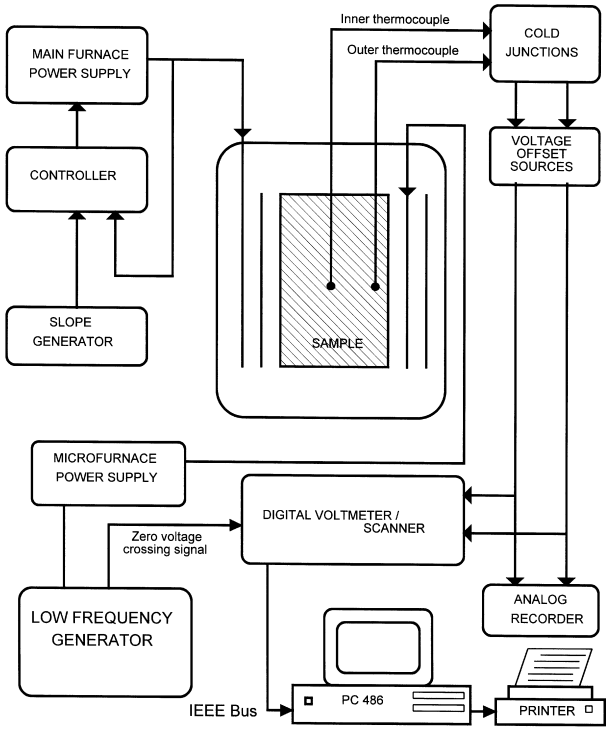

Fig. 2. Experimental setup.

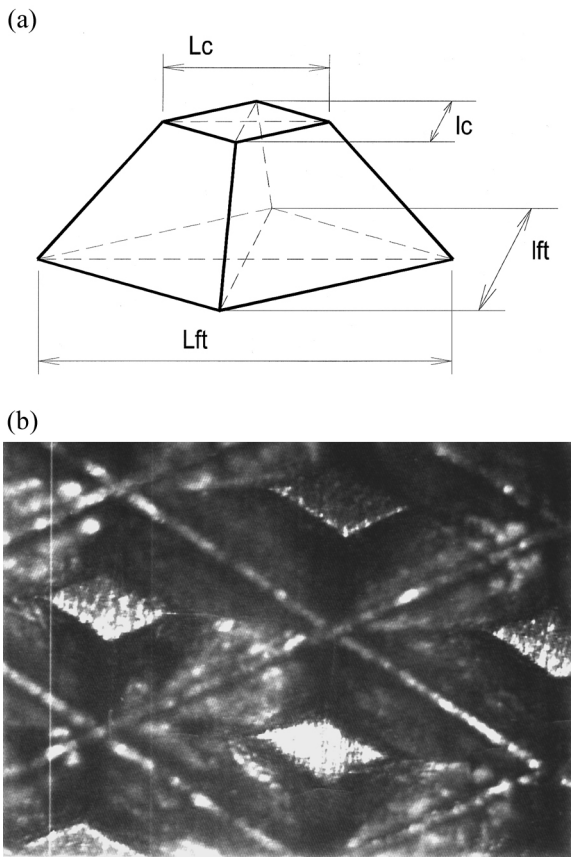

Fig. 3. Macroroughness of the interface. (a) Pyramidal asperity, (b) surface of the inner cylinder.

top and the bottom of the sample are insulated by some alumina disks as described in [14].

3.2. Sample description

The composite cylindrical sample (Fig. 1) is built from two concentric cylinders of 99 wt% pure nickel. The surface of the inner cylinder is knurled and exhibits truncated pyramidal macroasperities of rhombus section (Fig. 3) and 4.5×10^{-4} m height. Hence, the valleys between the asperities have a triangular profile. The surface of the outer cylinder is smooth in comparison with the inner one. After the knurling process, the outer diameter of the inner cylinder is 2×10^{-5} m greater than the inner diameter of the hollow cylinder. The inner cylinder is then contracted by liquid nitrogen cooling and inserted into the hollow one. The sample is cut in various thicknesses disks (Fig. 1). The stack configuration makes the drilling of the thermocouples holes easier.

Each thermocouple wire is spot-welded to the sample at the bottom of its hole. The whole part of the sample which is between the positive and negative wires welds of each thermocouple acts as the hot junctions of the thermoelectric circuit (Fig. 1). Obviously, this setup only works on electrical conductors; it brings the following improvements:

- the diameter of the required holes is lowered. Even if four holes are needed instead of two, the overall disturbance of the thermal field is smaller than in the two holes configuration, hence, experimental conditions are closer to the hypothesis of a homogeneous cylinder.
- if the regions between the welds of the positive and negative wires are isothermal, the thermocouples give this temperature, otherwise a temperature intermediate between the temperatures of the two welds is obtained. The thermal contact between the bead of the thermocouple and the sample is improved, the thermocouple temperature is then closer to the sample temperature. This point is theoretically and experimentally demonstrated by Cassagne et al. [16] in the frame of surface temperature measurements.

3.3. Phase change results

The amplitude decay measurements were not used since the signal to noise ratio was not good enough. Only phase change results are presented. The measurements were performed under vacuum at 865 K and under a pressure of 1.5×10^5 Pa of pure argon at 785 K and of pure helium at 750 K. The phase change of the wave is plotted versus the period (Fig. 4) for the three different experimental conditions. For the same thermocouple distance ($b = 0.015$ m), calculated isodiffusivity curves in the range (0.07×10^{-4}–0.11×10^{-4} $m^2\ s^{-1}$) are also plotted in Fig. (4). The diffusivity of a 99 wt% pure nickel lies within the range 0.11×10^{-4}–0.14×10^{-4} $m^2\ s^{-1}$ at 750 K, and increases with the temperature up to 0.12×10^{-4}–0.15×10^{-4} $m^2\ s^{-1}$ at 865 K. Hence, Fig. (4) shows off that the observed phase changes are higher than those which would be obtained for a massive nickel sample of similar purity. This is a clear evidence of the effect of the contact conductance.

The increase in the scattering of the data, as the period is lowered, is a direct consequence of the decrease of the amplitude of the signal; for a given distance, short periods thermal waves are damped stronger than long periods ones. Moreover, the signal originating from the microfurnace is more attenuated under argon and obviously under vacuum than under helium, the thermal conductivity of which is higher. This is the reason why the results under vacuum and under argon are so scattered. Finally, only the data obtained under helium have been used.

The thermal capacity, the density of the sample, the distances a and b are known quantities. The conductivity can be calculated from the diffusivity, the capacity and the density. However, the diffusivity of the sample is not known accurately, hence, Eq. (26) is an equation in two unknowns: the contact conductance and the diffusivity. As only phase information is avail-

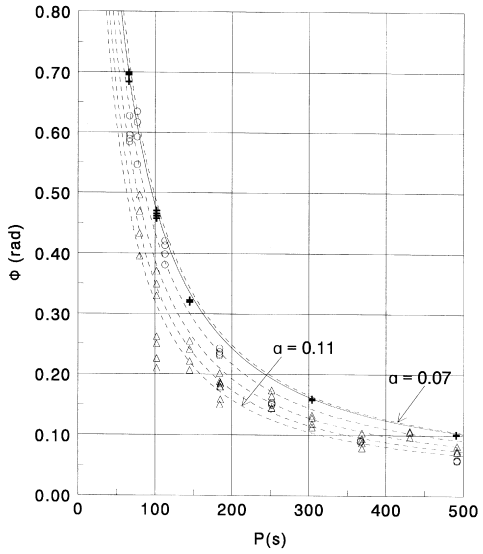

Fig. 4. Phase change vs. period. ◆: helium, 750 K. +: argon, 785 K. O: vacuum, 865 K. —: fit of the results under helium atmosphere. - - - -: isodiffusivity curves for the pure nickel, $\alpha = 7 \times 10^{-4}$, 8×10^{-4}, 9×10^{-4}, 10×10^{-4} and 11×10^{-4} $m^2\ s^{-1}$.

able, a single measurement is not sufficient to find the two unknowns, it is necessary to use the measurements set as a whole to achieve the best accuracy in the identification process.

3.4. The data reduction method and conductance results

The aim is to work out both, the unknown parameters α and h from the data reported in Fig. (4) by a fit following the two parameters non-linear model Eqs. (26)–(28). The non-linear least square fit is handled by the Levenberg–Marquardt algorithm [17] based on the χ^2 minimization:

$$\chi^2(\vec{p}) = \sum_{i=1}^{N} \left(\frac{\Phi_i - \Phi(P_i, (\alpha, h))}{\sigma_i} \right)^2 \quad (30)$$

where (P_i) are the various periods and (σ_i) the corresponding standard deviations.

The algorithm implements a double strategy: near the minimum, the parameters variation is approximated by a quadratic form (inverse Hessian method) while, far from the minimum, the steepest slope method is used. Moreover, if the random measurement error of each point is uncorrelated with the model, the Hessian matrix can be simply calculated from the first derivatives of the model with respect to the parameters. The calculations of the second derivatives are not necessary.

The mathematical developments leading to the numerical calculation of Eq. (26) and of the first derivatives versus h and α are reported in the Appendix.

As it can be seen in Fig. (4), the standard deviation (σ_i) is small as the period is great. For each period (P_i), considering that (i) the χ^2 minimisation is based on the assumption that random errors follow a normal distribution and (ii) an unbiased estimator of (σ_i) is given by $\Delta\Phi/m$ where $\Delta\Phi$ represents the sample width and m is a parameter which depends on the number of values in the sample [18]. The phase change measurements under helium and the corresponding results of the (σ_i) estimation procedure are presented in Table 1.

Table 1
Phase change measurements under helium atmosphere and standard deviation estimation

Period (s)	66.4	102.1	145.4	303.7	491.4
Φ_i (rad)	0.6966	0.4615	0.3193	0.1601	0.1015
	0.6995	0.4574	0.3226	0.1582	0.1016
	0.6841	0.4702	0.3209	0.1586	0.1004
	0.6954	0.4654		0.1579	0.1014
$\Delta\Phi$ (rad)	0.0154	0.0128	0.0033	0.0022	0.0012
σ_i estimated (rad)	0.0075	0.0062	0.0019	0.0011	0.0006

Three minimizations are performed. At first a two parameters fit, and then two fits of the conductance at constant diffusivities are chosen at the limits of the interval (0.11×10^{-4}–0.14×10^{-4} m^2 s^{-1}).

The results are presented in Table 2. In the first fit the adjusted diffusivity value 0.116×10^{-4} m^2 s^{-1} is consistent with the range (0.11×10^{-4}–$0.14\ 10^{-4}$ m^2 s^{-1}).

3.5. Error due to the uncertainties on the distances a and b

The maximum height of the asperities is 4.5×10^{-4} m. The absolute error in the distance between the axis of the cylindrical sample and the interface is $\Delta a = \pm 2.25 \times 10^{-4}$ m. The distance between the thermocouples is 1.5×10^{-2} m, the diameter of the thermocouples is 1×10^{-3} m. The absolute error on the location of the outer thermocouple is $\Delta b = \pm 5 \times 10^{-4}$ m. The errors which are induced in the conductance by Δa and Δb are calculated in Table 3.

In the error calculations, the possible erroneous location of the inner thermocouple is not taken into account. Actually, a displacement of this thermocouple to $r \neq 0$ modifies the analytical expression (Eq. (26)) of the phase change. As a consequence, an error calculation like the one that was done to estimate the error due to a change in the distance b is not straightforward. Simple overestimation of the total error is given by increasing twofold the outer thermocouple error because, in cylindrical geometry, two isophase curves around the location r are all the nearer that r is higher [19]. Hence, a displacement of the inner thermocouple yields a smaller error than a displacement of the outer thermocouple.

4. Comparison with a conductance model

The surface of the inner cylinder exhibits macroasperities distributed periodically. In this geometry, the thermal field can be split into n identical flux tubes. The heat equation can be solved inside an elementary flux tube. The resistances of all the tubes are combined in parallel to yield the total resistance of the interface.

Table 2
Fit of the parameters relative to the measurements under helium

Parameter	$10^4\alpha$ (m^2 s^{-1})	$10^{-4}h$ (W m^{-2} K^{-1})	χ^2
α and h	**0.116**	**1.05**	143
h	0.11	**1.16**	144
h	0.14	**0.815**	146

In the model [20], the interface is a plane and the flux tubes are cylinders. The thermal contact resistance can be written as a function of the ratio S^* between the contact area and the cross section of the elementary flux tube:

$$R_s = \frac{\sqrt{\pi}}{2 \cdot \lambda_s \sqrt{S^* \cdot n}} \cdot \left(1 - 1.41 \cdot \sqrt{S^*}\right) + \frac{2 \cdot d}{S^* \cdot \lambda_s} \cdot (1 - S^*)$$

where n is the number of the flux tubes per unit area, λ_s is the harmonic mean of the conductivities, $(2/\lambda_s = 1/\lambda_I + 1/\lambda_{II})d$ is the mean height of the asperities weighted by the conductivities:

$$d = \frac{\lambda_I \cdot \delta_I + \lambda_{II} \cdot \delta_{II}}{\lambda_I + \lambda_{II}}$$

where δ_I and δ_{II} are the height of the asperities in materials I and II, respectively. In the nickel/nickel sample, only the inner cylinder is knurled then $\lambda_s = \lambda$, $\delta_{II} = 0$ and $d = \delta/2$ where δ is the average height of the asperities.

Four parameters are needed to calculate the thermal resistance: the conductivity of the material, the asperities height, the solid/solid contact area and the elementary flux tube area.

The asperities have the shape of a truncated pyramid, the base of which is a rhombus (Fig. 3). The base of the pyramid is the flux tube area. The area of the top of the pyramid is the solid/solid contact area. This area is parallel to the base. The diagonals of the flux tube are denoted by L_{ft} and l_{ft}, the diagonals of the contact area are denoted by L_c and l_c. The numerical values of the diagonals are measured from a photograph of the surface of the inner cylinder and corrected to verify the geometrical relation:

$$l_c/l_{ft} = L_c/L_{ft}$$

.

$L_{ft} = 3 \times 10^{-3}$ m, $l_{ft} = 17 \times 10^{-4}$ m, $L_c = 8.6 \times 10^{-4}$ m and $l_c = 4.8 \times 10^{-4}$ m.

$S_{ft} = 2.6 \times 10^{-6}$ m^2 and $S_c = 21 \times 10^{-8}$ m^2. The ratio of the areas S_c/S_{ft} equals 0.081.

The number of the flux tubes per unit area: $n = S_{ft}^{-1} = 38 \times 10^4$ flux tubes m^{-2}.

The valleys between the asperities exhibit a triangular profile. Hence, if the curvature of the interface is neglected, the average height of the asperities ($\delta = 2.25 \times 10^{-4}$ m) is half the maximum height (4.5×10^{-4} m). The conductance by solid/solid contact is calculated for three diffusivity values in Table 4.

On the assumption that a perfect thermal contact is established between the asperities. The contribution λ_f of the intersticial medium to the total conductance of the interface is overestimated by: $\lambda_f = \lambda_{gas}/\delta$. Actually, this formula is valid only if the solid/solid contact area is neglected. To the extent that the mean height of the asperities is very much greater than the gas mean free path and that the gas pressure is greater than 10^5 Pa, the gas accommodation effect is negligible. The thermal conductivity of helium at 750 K and 10^5 Pa is 0.292 W m^{-1} K^{-1} [21]. The total contact conductance h is the sum of the two contributions $1/R_s$ and λ_f (Table 4).

Tables 2 and 4 show off that a good agreement is achieved between the measured and the calculated conductances when the diffusivity and the conductance are adjusted simultaneously. When the diffusivity is held constant ($\alpha = 0.11 \times 10^{-4}$ or 0.14×10^{-4} m^2 s^{-1}) and according to the identification procedure, the discrepancy lies within the range 8–40%. These observations tend to confirm that the diffusivity of the sample is close to 0.116×10^{-4} m^2 s^{-1}.

The discrepancy between the measurements and the model can have several origins. The experimental errors have been quantified in the former paragraph, the curvature of the sample interface is neglected in the model and the expression of the constriction function in the model is relevant to circular contact spots,

Table 3
Errors on the conductance due to the uncertainties on a and b

$10^4\alpha$ (m^2 s^{-1})	a (m)	b (m)	$10^{-4}h$ (W m^{-2} K^{-1})	$\Delta h/h$ (%)
0.11	**0.013**	**0.015**	**1.14**	0
0.11	0.013	0.0155	1.31	+14.9
0.11	0.013	0.0145	1.01	−11.4
0.11	0.013225	0.015	1.16	+1.75
0.11	0.012775	0.015	1.12	−1.75
0.14	**0.013**	**0.015**	**0.793**	0
0.14	0.013	0.0155	0.857	+8.07
0.14	0.013	0.0145	0.741	−6.56
0.14	0.013225	0.015	0.808	+1.89
0.14	0.012775	0.0155	0.779	−1.76

Table 4
Conductances calculated with the model

$10^4\alpha$ ($m^2\ s^{-1}$)	$10^{-3}C_p$ ($J\ kg^{-1}\ K^{-1}$)	$10^{-2}\lambda$ ($W\ m^{-1}\ K^{-1}$)	$10^{-4}/R_s$ ($W\ m^{-2}\ K^{-1}$)	$10^{-4}\lambda_f$ ($W\ m^{-2}\ K^{-1}$)	$10^{-4}h$ ($W\ m^{-2}\ K^{-1}$)
0.11	0.53	0.52	0.93	0.13	**1.06**
0.116	0.53	0.55	0.99	0.13	**1.12**
0.14	0.53	0.66	1.18	0.13	**1.31**

hence, in the present case a shape factor should be introduced.

Moreover, the knowledge of the thermal properties of the materials in contact is very important because simultaneous identification of the conductance and the diffusivities is not always possible and depends on the random errors on the phase change. The number of phase change measurements at a given frequency and the number of frequencies should be increased to improve the confidence in the statistical reduction method. Modifications of the experimental setup allowing to increase the spatial resolution of the temperature measurements are now under investigation.

Nevertheless, the orders of magnitude of the measurement and of the model agree well, which was the first goal of this preliminary work.

Acknowledgements

The authors are very grateful to Pr. Bardon (Université de Nantes) for valuable discussion.

Appendix A. Explicit analytical expressions of the phase change and its first derivatives

The phase change (Eq. (26)) is defined by: $\Phi = -\mathrm{Arg}(A)$,where

$$A = \frac{\theta(b)\cdot Bi}{(e\cdot a)^2 i\cdot I'_a\left(I'_a\cdot K_b - I_b\cdot K'_a\right) + Bi\cdot I_b}.$$

The complex Bessel functions are to be expanded into their real and imaginary parts using the Kelvin functions [22], to calculate $\mathrm{Arg}(A)$. The Kelvin functions (ber, bei, ker, kei) and their first derivatives (ber′, bei′, ker′, kei′) are numerically calculated using polynomial approximations [22]. The Kelvin functions of order 1 (ber_1, bei_1, ker_1, kei_1) are linear combinations of the first derivatives [22]. The second derivatives (ber″, bei″, ker″, kei″) are obtained by derivation of the polynomial approximations of the first derivatives.

Let exp1 to exp5, RE and IM be auxiliary expressions such that:

$$\exp 1 = 2\cdot \mathrm{ber}_1(e\cdot a)\cdot \mathrm{bei}_1(e\cdot a)$$

$$\exp 2 = \mathrm{ber}_1^2(e\cdot a) - \mathrm{bei}_1^2(e\cdot a)$$

$$\exp 3 = \mathrm{bei}_1(e\cdot a)\cdot \mathrm{kei}_1(e\cdot a) - \mathrm{ber}_1(e\cdot a)\cdot \mathrm{ker}_1(e\cdot a)$$

$$\exp 4 = \mathrm{ber}_1(e\cdot a)\cdot \mathrm{kei}_1(e\cdot a) + \mathrm{bei}_1(e\cdot a)\cdot \mathrm{ker}_1(e\cdot a)$$

$$\mathrm{RE} = \exp 1\cdot \mathrm{ker}(e\cdot b) + \exp 2\cdot \mathrm{kei}(e\cdot b) + \exp 3\cdot \mathrm{bei}(e\cdot b) - \exp 4\cdot \mathrm{ber}(e\cdot b)$$

$$\mathrm{IM} = \exp 1\cdot \mathrm{kei}(e\cdot b) - \exp 2\cdot \mathrm{ker}(e\cdot b) - \exp 3\cdot \mathrm{ber}(e\cdot b) - \exp 4\cdot \mathrm{bei}(e\cdot b)$$

$$\exp 5 = \frac{(e\cdot a)^2\cdot \mathrm{IM} + Bi\cdot \mathrm{bei}(e\cdot b)}{(e\cdot a)^2\cdot \mathrm{RE} + Bi\cdot \mathrm{ber}(e\cdot b)}$$

The phase change is then given by:

$$\Phi = \tan^{-1}(\exp_5)$$

The derivative with respect to the conductance is given by:

$$\frac{\partial \Phi}{\partial h} = \frac{1}{1+\exp 5^2}\cdot\frac{a}{\rho\cdot C_p\cdot\alpha}\cdot\frac{(e\cdot a)^2\cdot(\mathrm{RE}\cdot \mathrm{bei}(eb) - \mathrm{IM}\cdot \mathrm{ber}(eb))}{\left((e\cdot a)^2\cdot \mathrm{RE} - Bi\cdot \mathrm{ber}(eb)\right)^2}$$

With the following expressions:

$$\mathrm{BR2A} = \frac{\mathrm{ber}''(e\cdot a) - \mathrm{bei}''(e\cdot a)}{\sqrt{2}}$$

$$\mathrm{BI2A} = \frac{\mathrm{ber}''(e\cdot a) + \mathrm{bei}''(e\cdot a)}{\sqrt{2}}$$

$$\mathrm{KR2A} = \frac{\mathrm{ker}''(e\cdot a) - \mathrm{kei}''(e\cdot a)}{\sqrt{2}}$$

$$\mathrm{KI2A} = \frac{\mathrm{ker}''(e\cdot a) + \mathrm{kei}''(e\cdot a)}{\sqrt{2}}$$

$$\exp 1' = -\frac{e\cdot a}{\alpha}\cdot(\mathrm{ber}_1(e\cdot a)\cdot \mathrm{BI2A} + \mathrm{bei}_1(e\cdot a)\cdot \mathrm{BR2A})$$

$$\exp 2' = -\frac{e\cdot a}{\alpha}\cdot(\mathrm{ber}_1(e\cdot a)\cdot \mathrm{BR2A} - \mathrm{bei}_1(e\cdot a)\cdot \mathrm{BI2A})$$

$$\exp 3' = -\frac{e\cdot a}{2\cdot\alpha}\cdot(\mathrm{kei}_1(e\cdot a)\cdot \mathrm{BI2A} + \mathrm{bei}_1(e\cdot a)\cdot \mathrm{KI2A} - \mathrm{ker}_1(e\cdot a)\cdot \mathrm{BR2A} - \mathrm{ber}_1(e\cdot a)\cdot \mathrm{KR2A})$$

$$\exp 4' = -\frac{e\cdot a}{2\cdot\alpha}\cdot(\mathrm{kei}_1(e\cdot a)\cdot \mathrm{BR2A} + \mathrm{ber}_1(e\cdot a)\cdot \mathrm{KI2A} + \mathrm{ker}_1(e\cdot a)\cdot \mathrm{BI2A} + \mathrm{bei}_1(e\cdot a)\cdot \mathrm{KR2A})$$

$$\mathrm{RE}' = -\frac{e\cdot b}{2\cdot\alpha}\cdot\big(\exp 1\cdot \mathrm{ker}'(e\cdot b) + \exp 2\cdot \mathrm{kei}'(e\cdot b) + \exp 3\cdot \mathrm{bei}'(e\cdot b) - \exp 4\cdot \mathrm{ber}'(e\cdot b)\big) + \exp 1' \cdot \mathrm{ker}(e\cdot b) + \exp 2'\cdot \mathrm{kei}(e\cdot b) + \exp 3'\cdot \mathrm{bei}(e\cdot b) - \exp 4'\cdot \mathrm{ber}(e\cdot b)$$

$$\mathrm{IM}' = -\frac{e\cdot b}{2\cdot\alpha}\cdot\big(\exp 1\cdot \mathrm{kei}'(e\cdot b) - \exp 2\cdot \mathrm{ker}'(e\cdot b) - \exp 3\cdot \mathrm{ber}'(e\cdot b) - \exp 4\cdot \mathrm{bei}'(e\cdot b)\big) + \exp 1' \cdot \mathrm{kei}(e\cdot b) - \exp 2'\cdot \mathrm{ker}(e\cdot b) - \exp 3'\cdot \mathrm{ber}(e\cdot b) - \exp 4'\cdot \mathrm{bei}(e\cdot b)$$

$$\exp 5' = (e\cdot a)^2\cdot\left(\mathrm{RE}' - \frac{\mathrm{RE}}{\alpha}\right)$$

$$\exp 7' = (e\cdot a)^2\cdot\left(\mathrm{IM}' - \frac{\mathrm{IM}}{\alpha}\right)$$

$$\exp 6 = \big((e\cdot a)^2\cdot\mathrm{RE} + Bi\cdot\mathrm{ber}(e\cdot b)\big)\cdot\left((e\cdot a)^2\cdot\left(\mathrm{IM}' - \frac{\mathrm{IM}}{\alpha}\right) - \frac{Bi\cdot e\cdot b}{2\cdot\alpha}\cdot\mathrm{bei}'(e\cdot b) - \frac{\lambda_c\cdot a}{\rho\cdot C_p\cdot\alpha^2}\cdot\mathrm{bei}(e\cdot b)\right) - \big((e\cdot a)^2\cdot\mathrm{IM} + Bi\cdot\mathrm{bei}(e\cdot b)\big)\cdot\left((e\cdot a)^2\cdot\left(\mathrm{RE}' - \frac{\mathrm{RE}}{\alpha}\right) - \frac{Bi\cdot e\cdot b}{2\cdot\alpha}\cdot\mathrm{ber}'(e\cdot b) - \frac{\lambda_c\cdot a}{\rho\cdot C_p\cdot\alpha^2}\cdot\mathrm{ber}(e\cdot b)\right)$$

The derivative with respect to the diffusivity is given by:

$$\frac{\partial\Phi}{\partial\alpha} = \frac{1}{1+\exp 5^2}\cdot\frac{\exp 6}{\big((e\cdot a)^2\cdot\mathrm{RE} - Bi\cdot\mathrm{ber}(eb)\big)^2}$$

References

[1] L.S. Fletcher, Recent developments in contact conductance heat transfer, ASME Journal of Heat Transfer 110 (1988) 1059–1070.

[2] M. Laurent, J.L. Macqueron, A. Gery, G. Sinicki, Thermodynamique: La méthode du signal bref appliquée à la mesure des résistances thermiques de contact, C. R. A. S. Paris B265 (2) (1967) 1369–1371.

[3] A.J. Angström, Neue Methode das Wärmeleitungsvermögen der Körper zu Bestimmen, Annalen der Physic und Chemie 114 (1861) 513–530.

[4] C. Saint Blanquet, J.P. Bardon, Etude des transferts de chaleur entre solides accolés en régime thermique sinusoïdal, C. R. A. S. Paris B273 (1971) 109–112.

[5] N.J. Robinson, M. Tomsic, Thermal contact resistance by reflection of heat diffusion waves, Nuclear Technology 12 (4) (1971) 393–403.

[6] H. Cordier, J.C. Payrault, J.J. Vullierme, Etude de l'influence des résistances thermiques de contact sur les transferts de chaleur entre matériaux accolés dans les phénomènes transitoires, Entropie 65 (1975) 20–29.

[7] T. Nguyen-Minh, G. Neuer, Measurement of thermal gap resistance and contact resistance by the modulated heating method, High Temp. High Press 13 (1981) 113–118.

[8] R.D. Cowan, Proposed method of measuring thermal diffusivity at high temperatures, Journal of Applied Physics 32 (7) (1961) 1363–1370.

[9] G.M. Ayers, L.S. Fletcher, C.V. Madhusudana, Thermal contact conductance of composite cylinders, J. of Thermophysics and Heat Transfer 11 (1) (1997) 72–81.

[10] A. Degiovanni, Yin Zhang Xiaojing, Modèle de résistances thermiques de contact entre deux surfaces cylin-

driques: approche microscopique 3D, Int. J. Heat Mass Transfer 41 (3) (1998) 601–612.
[11] C.V. Madhusudana, A.L. Litvak, Thermal contact conductance of composite cylinders: an experimental study, J. of Thermophysics 4 (1) (1990) 79–85.
[12] B. Fourcher, J.P. Bardon, H. Mallard, Transfert de chaleur en régime périodique à l'interface de deux milieux: Problèmes posés par l'ecriture des conditions aux limites classiques, Entropie 64 (1975) 11–26.
[13] N.W. Mac Lachlan, Bessel Functions for Engineers, 2nd ed., Clarendon Press, Oxford, England, 1955, p. 204 (formula 219).
[14] J. Khedari, P. Benigni, J. Rogez, J.C. Mathieu, New apparatus for thermal diffusivity measurements of refractory solid materials by the periodic stationary method, Rev. of Sc. Instr. 66 (1) (1995) 193–198.
[15] J. Khedari, P. Benigni, J. Rogez, J.C. Mathieu, A solution of the heat conduction equation in the finite cylinder exposed to periodic boundary conditions: the case of steady oscillation and constant thermal properties, Proc. R. Soc. Lond. A 438 (1992) 319–329.
[16] B. Cassagne, J.P. Bardon, J.V. Beck, Theoretical and experimental analysis of two surfaces thermocouples, in: 8th Int. Conf. of Heat Transfer, 1986, San Francisco, 1992, pp. 483–488.
[17] W.H. Press, B.P. Flannery, S.A. Teukolsky, W.T. Vetterling, Numerical Recipes, Cambridge University Press, Cambridge, 1988.
[18] CEA, Statistique appliquée à l'exploitation des mesures, 1, Masson ed., 1978, p. 70 and p. 51 of the tables session.
[19] J. Khedari, Mesure de diffusivité thermique à haute température par une méthode périodique et étude de transfert thermique en géométrie cylindrique, Thesis, Université de Provence Aix-Marseille I, 1990.
[20] J.P. Bardon, Introduction à l'étude des résistances thermiques de contact, Revue Générale de Thermique Française 125 (5) (1972) 429–447.
[21] R.W. Powell, C.Y. Ho, P.E. Liley, in: R.C. Weast (Ed.), Handbook of Chemistry and Physics, 54th ed., CRC Press, Boca Raton, 1973/74.
[22] M. Abramowitz, I.A. Stegun, Handbook of Mathematical Functions, 9th ed., Dover Pub. Inc, New York, 1970.